AIP | The Journal of Chemical Physics

Solvation of fluoro-acetonitrile in water by 2D-IR spectroscopy: A combined experimental-computational study

Pierre-André Cazade, Halina Tran, Tristan Bereau, Akshaya K. Das, Felix Kläsi, Peter Hamm, and Markus Meuwly

Citation: The Journal of Chemical Physics **142**, 212415 (2015); doi: 10.1063/1.4916630
View online: http://dx.doi.org/10.1063/1.4916630
View Table of Contents: http://scitation.aip.org/content/aip/journal/jcp/142/21?ver=pdfcov
Published by the AIP Publishing

Solvation of fluoro-acetonitrile in water by 2D-IR spectroscopy: A combined experimental-computational study

Pierre-André Cazade,[1,a)] Halina Tran,[2,a)] Tristan Bereau,[3] Akshaya K. Das,[1] Felix Kläsi,[2] Peter Hamm,[2] and Markus Meuwly[1,4,b)]
[1]*Department of Chemistry, University of Basel, Klingelbergstrasse 80, 4056 Basel, Switzerland*
[2]*Department of Chemistry, University of Zurich, Winterthurerstr. 190, 8057 Zurich, Switzerland*
[3]*Max-Planck-Institut für Polymerforschung, Ackermannweg 10, 55128 Mainz, Germany*
[4]*Department of Chemistry, Brown University, Providence, Rhode Island 02912, USA*

(Received 13 February 2015; accepted 16 March 2015; published online 7 April 2015)

The solvent dynamics around fluorinated acetonitrile is characterized by 2-dimensional infrared spectroscopy and atomistic simulations. The lineshape of the linear infrared spectrum is better captured by semiempirical (density functional tight binding) mixed quantum mechanical/molecular mechanics simulations, whereas force field simulations with multipolar interactions yield lineshapes that are significantly too narrow. For the solvent dynamics, a relatively slow time scale of 2 ps is found from the experiments and supported by the mixed quantum mechanical/molecular mechanics simulations. With multipolar force fields fitted to the available thermodynamical data, the time scale is considerably faster—on the 0.5 ps time scale. The simulations provide evidence for a well established CF–HOH hydrogen bond (population of 25%) which is found from the radial distribution function $g(r)$ from both, force field and quantum mechanics/molecular mechanics simulations. © *2015 AIP Publishing LLC*. [http://dx.doi.org/10.1063/1.4916630]

I. INTRODUCTION

Despite their importance, little is known about the energetics and dynamics of protein-ligand complexes involving halogenated, pharmaceutically active compounds. In particular, fluorine often replaces hydrogen in organic molecules but the size and stereoelectronic influences of the two atoms are quite different. Typical examples for top-selling fluorinated pharmaceuticals include the antidepressant fluoxetine (Prozac),[1] the cholesterol-lowering drug atorvastatin (Lipitor),[2] and the antibacterial ciprofloxacin (Ciprobay).[3] Electronegativity considerations would suggest that —CF behaves similarly to —CO and —CN fragments. On the other hand, the —CF unit, that is organic F, has a low proton affinity and is weakly polarizable. The large number of —CF$\cdots$HX— (where X = O, N, S) as well as —CF$\cdots$HC— contacts found in the Cambridge Structural Database (CSD) point to the fact that it is favorable for the –CF dipole to engage in directional intermolecular interactions.[4] Furthermore, recently, synthetic work on trifluoroborates established H-bonding between the fluorines and the NH groups of a 1,3,5-trisubstituted 2,4,6-triethylbenzene scaffold.[5]

An experimental approach to study the solvation of —CF groups in water is provided by two-dimensional infrared (2D-IR) spectroscopy, which is a powerful experimental technique that can reveal detailed information on the structure and dynamics of condensed-phase systems.[6] In the context of the present problem, 2D-IR spectroscopy can elucidate the lineshape function of a given vibrational mode in much more detail than just conventional IR absorption spectroscopy (1D-IR spectroscopy), including its inhomogeneous broadening as well as spectral diffusion. That is, due to the interaction of the corresponding IR chromophore with its solvent environment, spectral shifts are induced that lead to an instantaneous inhomogeneous distribution of absorption frequencies, as each molecule in the ensemble will be surrounded by a slightly different solvent cage. However, since the solvent is dynamic, that inhomogeneous distribution is not static, so the frequency of a given molecule will be modulated as a function of time, a process called spectral diffusion. The timescale of spectral diffusion, which can be measured directly with 2D-IR spectroscopy via the tilt of the 2D-IR lineshapes,[7–9] is related to the timescale of interchanging solvent structures. If an IR chromophore is hydrogen bonded to the solvent, one expects that the inhomogeneous width increases with stronger hydrogen bonding and the timescale of spectral diffusion reflects the hydrogen bond lifetime. That type of experiment has been performed on various vibrational chromophores, such as the N_3^- (Ref. 10) or the CN^- (Refs. 11 and 12) ion in water, the —C═O group of N-methylacetamide (NMA) in water,[13,14] the phosphate group of hydrated phospholipids,[15] the OH/OD vibration of HOD in either D_2O or H_2O,[16–19] —C≡O, —C≡N, —N_3^- or —SCN ligands,[20–24] or as unnatural amino acids[25–28] inside proteins, to name just a few.

A strength of 2D-IR spectroscopy is the fact that the experimental results can be compared in a relatively straightforward manner with all-atom molecular dynamics (MD) simulations. In that way, one can first extract a microscopic picture of the underlying processes giving rise to spectral

a)P.-A. Cazade and H. Tran contributed equally to this work.
b)Author to whom correspondence should be addressed. Electronic mail: m.meuwly@unibas.ch

diffusion, and second validate and/or further improve the force fields. In addition, once validated, the simulations provide the opportunity for further in-depth analysis and understanding of the atomic and molecular motions which are responsible for the observed time scales.[29] Essentially two approaches have been pursued to perform such simulations: (a) running an MD simulation with a standard force field in order to sample the conformational space and then calculating instantaneous frequency shifts of the chromophore of interest, utilizing maps that have typically been pre-calculated on a higher *ab-initio* level of theory,[30–33] or (b) developing better, physics-based empirical force fields that are used for both the MD trajectory and the spectral calculation in a consistent manner.[29,34] For cyanide in water, a force field that correctly describes solvation free energies, vibrational relaxation and the 1-dimensional spectroscopy was found to closely match the experimentally measured spectral diffusion dynamics.[29] For the case of NMA solvated in water a force field reproducing thermodynamic data from experiment was found to lead to somewhat faster dynamics (around 1 ps compared to between 1 and 1.6 ps, depending on the experiment).[13,14,34]

This second approach attempts to treat the dynamics and computation of a physico-chemical observable on the same footing. One of the reasons why this is desirable is the situation in which computer simulations are unable to correctly describe experimental data because under such circumstances the question whether the sampling or scoring of the property is insufficient does not arise. In other words, if the dynamics and the computation of the property (or properties) are based on the same force field, it is likely that an improved description of the intermolecular interactions will provide a better description of the underlying physics.

In the present work, the solvent structure and dynamics around the —CF group of fluorinated acetonitrile (FACN) in water (D_2O) is investigated spectroscopically and with atomistic MD simulations. That molecule was chosen because of its small size, the interesting chemical environment of a fluorinated group and the fact that mixed quantum mechanical/molecular mechanics simulations are possible. Furthermore, the molecule does not have different isomers, which would give rise to inhomogeneous broadening in addition to the solvent induced effects. And finally, the molecule was selected based on its somewhat larger (in comparison to other fluorinated compounds) absorption cross section together with the fact that dimerisation/aggregation occurs only at a rather high concentration. The combined experimental/theoretical study reveals that even with multipolar force fields benchmarked against available thermodynamic data, the solvent dynamics cannot be quantitatively captured compared to experiments, whereas semiempirical quantum mechanics/molecular mechanics (QM/MM) simulations provide a considerably improved description.

II. EXPERIMENTAL METHODS

Tunable femtosecond IR pulses centered around 1044 cm^{-1}, the frequency of the CF-stretch vibration of FACN dissolved in D_2O, were produced in a Ti:sapphire pumped optical parametrical amplifier (OPA).[35] A pump-probe version of a 2D-IR spectrometer has been used, employing an interferometer to generate two collinear phase-locked pump-pulses,[36] which were focused onto the sample with 150 μm spot size. Unwanted interference effects resulting from scattering were suppressed with the help of a wobbling Brewster window.[37] The probe beam was sent through a spectrograph onto a HgCdTe (MCT) array detector for frequency-resolved detection with a spectral resolution of 3 cm^{-1}/pixel in the probe frequency dimension. The coherence time was scanned between (−500, 1500) fs, revealing a resolution of 11 cm^{-1} in the pump-frequency dimension, and 2D-IR spectra were recorded for various population times up to 2 ps. The sample was dissolved in D_2O and sandwiched between two BaF_2 windows separated by 6 μm, both chosen to minimize the background absorption. To evaluate whether the sample is monomeric at the concentration used in the 2D-IR experiment, ^{1}H-NMR spectra have been measured in a Bruker AV2-500 (500 MHz) spectrometer.

All experiments were performed at room temperature. The OPA was operated at the low-frequency edge of its working range, resulting in a combined energy of only 0.1 μJ for both pump pulses, which generates a heat jump of $\lesssim$0.1 K.

III. COMPUTATIONAL METHODS

In the simulations using empirical force fields, a conventional point charge (PC), a multipole (MTP), and a fluctuating point charge (FPC) model was parametrized and employed. In addition, mixed quantum mechanics/molecular mechanics employing the self-consistent charges-density functional tight binding (SCC-DFTB) method were performed. For comparison, acetonitrile (ACN) without fluorination has been considered as well. The following summarizes the simulation methods together with the parametrizations for FACN and ACN.

A. Molecular dynamics simulations

All MD simulations were performed with CHARMM.[38] Point charges, Lennard-Jones (LJ), and torsion angle parameters for FACN are based on CGenFF.[39] Similarly, all bond parameters are those of CGenFF except for the CF bond r for which a Morse potential was used to account for anharmonicity. To that end the FACN structure is first optimized at the MP2/aug-cc-pVTZ level. Then, a scan along r is performed at the same level of theory. The energy of 16 points is computed on a grid including r = 1.079 Å to r = 2.579 Å in increments of 0.1 Å. For the same 16 structures, the energy provided by the CGenFF model involving all the parameters except for the CF bond is subtracted form the QM energy and is then fitted to a Morse potential $V(r) = D_0[1 - \exp(-\beta(r - r_0))]^2$ which yields parameters D_0 = 98.7 kcal/mol, r_0 = 1.3554 Å, and β = 2.1557 $Å^{-1}$. For water, the TIP3P model was used.[40] LJ interactions were computed with a 12 Å cutoff switched at 10 Å. For the MTP interactions, the monopoles are treated using Particle-Mesh Ewald (PME) with grid-size spacing of 1 Å, characteristic reciprocal length κ = 0.32 $Å^{-1}$, and interpolation order 6, while higher multipoles are treated with

a 12 Å cutoff and a force shifted damping function. For the PC model, a 12 Å cutoff with the force shifted function is used and simulations with PME with the treatment described above were also carried out for comparison. All bonds involving hydrogen atoms are constrained via the SHAKE algorithm.[41]

Condensed-phase simulations—FACN solvated in water or pure-liquid FACN for parametrizing the nonbonded parameters—were carried out in cubic boxes of approximately $30 \times 30 \times 30$ Å^3 size with a density corresponding to that at ambient temperature and pressure. Standard minimization, heating, and equilibration procedures for ~100 ps were employed to prepare the systems. Production simulations of 5 ns each for the spectroscopic observables were run in the *NVT* ensemble at 300 K using a velocity-Verlet integrator and a Nosé-Hoover thermostat. The timestep was Δt = 1.0 fs and snapshots were recorded every 5 steps.

For the parametrization of the MTP force field, simulations in the *NPT* ensemble with a Hoover heat-bath and pressure coupling were carried out.[42] These simulations were also run at T = 300 K, P = 1 atm, and the masses of the temperature and pressure piston to 20% and 2% of the system's mass, respectively. A Langevin damping coefficient $\gamma_p = 20$ ps^{-1} was applied on the piston to equilibrate the box size. Long-range corrections were applied to the Lennard-Jones interactions.[43]

B. Intermolecular interactions

For the production MD simulations with multipolar interactions the recently developed MTPL module[44] to compute MTP interactions in the atom's local frame was used.[45] Density, heat of vaporization, and hydration free-energy (from thermodynamic integration) calculations were performed as described previously.[44,46] The MTP coefficients were fitted to an *ab initio* electrostatic potential (ESP) obtained from MP2/aug-cc-PVDZ calculations. This level of theory has been used in recent work following the same parametrization protocol as that employed in the present work and differs from that for the PC model above.[44] Multiple conformations of FACN were included in the fit to allow for better parameter transferability.[45,47,48] To ensure consistency between the CGenFF PCs and the fitted MTPs, each monopole was constrained to deviate at most by an amount λ_{PC} from the reference value (i.e., provided by CGenFF). Effectively, larger values of λ_{PC} will provide more flexibility—and thus better fits—at the expense of consistency with the reference PCs.

Any modification to the electrostatics will *de facto* require a reparametrization of the LJ coefficients. A method to adjust the LJ coefficients to balance changes due to the electrostatics has recently been presented.[34] The reparametrization of the LJ interactions is achieved by monitoring three standard thermodynamic observables used in condensed-phase force-field parametrizations—pure-liquid density, ρ, heat of vaporization, ΔH_{vap}, and hydration free energy, ΔG_{hyd}. We vary the LJ radii of each atom type according to the strength of the associated MTP coefficients (i.e., stronger MTPs will tend to require a stronger LJ correction), yielding a single optimization parameter, λ_{LJ}, describing the relative increase in LJ radius, $R_{min}/2$. By systematically varying the free parameters λ_{PC} and λ_{LJ}, we search for the force field that faithfully reproduces the above mentioned thermodynamic quantities, see supplementary material.[58] For comparison, simulations for regular ACN were also carried out. To that end, MTP and PC models were parametrized following the same procedure as that for FACN (see supplementary material[58]).

A FPC model was also parametrized. FPCs have proved to be useful to describe the electron density as a molecule undergoes conformational changes[34] and to reproduce up to the quadrupole moment in diatomic molecules.[29,49,50] The nuclear charges are a function of the coordinate of interest, which is the CF bond length in the present case. From the electronic structure calculations for the CF-Morse potential described above, nuclear charges are fitted to the electrostatic field. For each atom, the charge as a function of the CF bond length is then fitted to a quadratic function $q_X = a_{X,0} + a_{X,1}r + a_{X,2}r^2$. The set of polynomial parameters is then slightly adjusted to ensure that the total charge of the molecule is zero for any CF bond length. The final parameters are reported in Table I.

In addition to the simulations with refined force fields, mixed QM/MM simulations were carried out. The FACN solute was treated with the SCC-DFTB method[51] whereas the surrounding solvent was described by TIP3P water. A thorough account of SCC-DFTB, the current implementation in CHARMM, and the parameters for halogenated species have been given previously.[51–53] Its highly attractive feature is that it provides reasonable accuracy, typically better than other semi-empirical approaches (e.g., AM1) at low computational cost (i.e., about 100–1000 times faster than a B3LYP/6-31G** calculation). The speedup is owed to approximations to the electronic Hamiltonian and the use of tabulated values for atom-pairwise matrix elements. Within a QM/MM simulation the QM/MM electrostatic energy consists of the MM partial charges interacting with the Mulliken charges on the atoms in the quantum part. For the van der Waals interactions, the MM atoms carry their usual van der Waals parameters whereas the QM atoms are assigned van der Waals parameters of the corresponding MM atom types.[52] The simulations were run for 5 ns with a time step of Δt = 0.25 fs to account for the rapid H-motion in FACN and frequencies $\omega(t)$ were determined in the same fashion as already described above from 10^6 snapshots.

C. Calculation of 2D-IR spectra

The details of the spectra calculation have been outlined in previous work,[34] and only a brief summary is provided here. The linear response function $R^{(1)}(t)$, as well as the 3rd-order rephasing and non-rephasing response functions

TABLE I. Parameters of the fluctuating point charge model for FACN.

X	a_0 (e)	a_1 (eÅ^{-1})	a_2 (eÅ^{-2})
C(CN)	−0.246 729	0.528 890	−0.117 053
N	−0.406 464	−0.066 787	0.043 196 2
C(CH$_2$F)	1.306 960	−1.060 410	0.229 191
H	−0.467 873	0.524 652	−0.103 226
F	0.281 979	−0.150 997	0.051 117 8

$R_r^{(3)}(t_3,t_2,t_1)$ and $R_{nr}^{(3)}(t_3,t_2,t_1)$, respectively, are determined from the frequency fluctuation correlation function (FFCF) within the framework of a cumulant expansion truncated at second order.[6,54] The anharmonic shift $\Delta = \omega_{01} - \omega_{12}$ between the fundamental and the first vibrationally excited state is set to 18 cm^{-1}, which is consistent with the experimental observations and the Morse potential used in the simulations.

The lineshape function and $g(t)$ is obtained from a double integration of the FFCF

$$g(t) = \int_0^t \int_0^{\tau'} d\tau' d\tau'' \langle \delta\omega_{01}(\tau'')\, \delta\omega_{01}(0)\rangle, \qquad (1)$$

where the FFCF, $C(t)$, is determined from the frequency trajectory $\omega(t)$ according to

$$\begin{aligned} C(t) &= \langle \delta\omega(t_0)\, \delta\omega(t_0+t)\rangle_{t_0} \\ &= \langle (\omega(t_0) - \overline{\omega})(\omega(t_0+t) - \overline{\omega})\rangle_{t_0}. \end{aligned} \qquad (2)$$

With that, the linear response function is defined as

$$R^{(1)}(t) \propto e^{-g(t)} \qquad (3)$$

and the corresponding terms for the third order response functions are given in Refs. 6 and 54. The short lifetime of the vibrationally excited state T_1 contributes significantly to the lineshapes. This is taken into account phenomenologically by multiplication of the linear response function with

$$\exp\left(-\frac{t}{2T_1}\right) \qquad (4)$$

together with the related factors for the third order response functions.[6] A value of $T_1 = 1.2$ ps is used, which has been deduced from experiment (see below). From the response functions, the associated absorption spectrum is calculated as a 1D Fourier transformation, and the 2D-IR spectra as 2D-Fourier transformations with respect to t_1 and t_3. Finally, purely absorptive 2D-IR spectra are calculated as a proper sum of rephasing and non-rephasing 2D-IR spectra.[6]

To obtain the frequency trajectory $\omega(t)$, instantaneous normal mode calculations of FACN are performed along the MD trajectory with the VIBRAN module in CHARMM. For each snapshot, FACN is minimized while the environment is kept in the configuration found in the trajectory, and the normal modes of FACN are calculated. Keeping the environment in its MD structure is necessary primarily to reflect the MD sampling and also to decouple the FACN normal modes from those of the solvent. This approach allows one to run a fully free dynamics, unlike the method used in a previous study,[34] where the solute molecule is frozen at its quantum gas phase structure.

IV. EXPERIMENTAL RESULTS

Figure 1, blue, shows the absorption spectrum of the CF-vibration of FACN in D_2O at the condition at which also the 2D-IR spectra are taken, that is, at 200 mM concentration and with a sample thickness of ≈6 μm. The band is centered at 1044 cm^{-1} with a peak absorption of only 8 mM and a width of 20 cm^{-1} (FWHM). From these numbers, a peak extinction coefficient of $\epsilon \approx 60$ $M^{-1}cm^{-1}$ can be estimated.

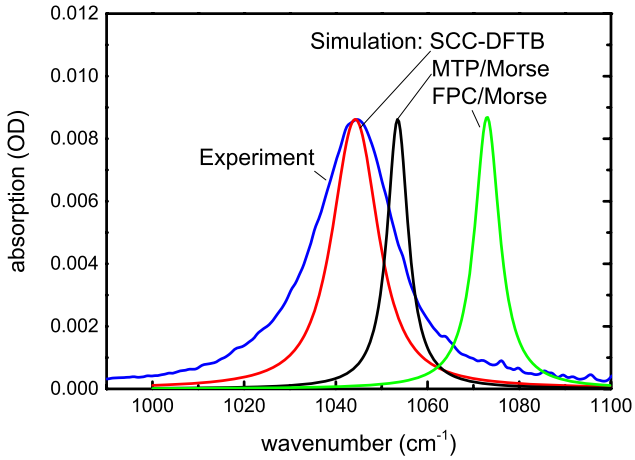

FIG. 1. Experimental absorption spectrum (blue) of the CF-vibration of FACN in D_2O with the background from water and the cuvette windows subtracted. The data were recorded at 200 mM concentration and with a sample thickness of ≈6 μm. The computed lineshapes from simulations with the PC (black) and MTP (red) models are shown together with the results from SCC-DFTB simulations (red). The computed spectra are normalized to the experimental one to facilitate comparison.

That small extinction coefficient together with the limited amount of IR light at the edge of the working range of the OPA[35] and the very large background absorption of the D_2O solvent (0.35 OD), originating from the wing of the D_2O bending mode and the onset of the water libration (see supplementary material, Figure S1),[58] required a rather high sample concentration. In order to evaluate to what extent the sample dimerizes/aggregates, ^{1}H-NMR spectra have been measured in dependence of concentration (see supplementary material, Figure S2).[58] These measurements revealed that a concentration of 200 mM is still close to the dilute limit, in the sense that FACN molecules essentially do not influence each other. That concentration has therefore been chosen for the 2D-IR experiments as a compromise between signal strength on the one hand and being close to the dilute limit on the other hand.

Figure 2 shows a sequence of experimental 2D-IR spectra with the population time varied between 100 fs and 2 ps. The Fourier transformation used to calculate the 2D spectrum suppresses any constant background that might originate from the water response (where it might helps that the water background, albeit being large, is relatively flat in the frequency range of the FACN vibration, see supplementary material, Figure S1).[58] It can be seen that the intensity of the peaks rapidly decreases as a result of vibrational relaxation. The maximum peak height is reported in Figure 3(a). A single exponential fit of these data reveals a time constant of 1.2 ± 0.06 ps, which lies in the expected range for vibrational relaxation in similar-sized molecules. The fast decay of the signal limits the time window, for which 2D-IR spectra can be observed, to ≈2 ps. In fact, the experimental data seem to deviate from an exponential decay after around 1.5-2 ps, which might originate from a long-lived contribution caused by heat induced frequency shifts of the —CF band and/or residual scattering.

The most important property of the 2D-IR spectra shown in Figure 2, which can be directly compared to the

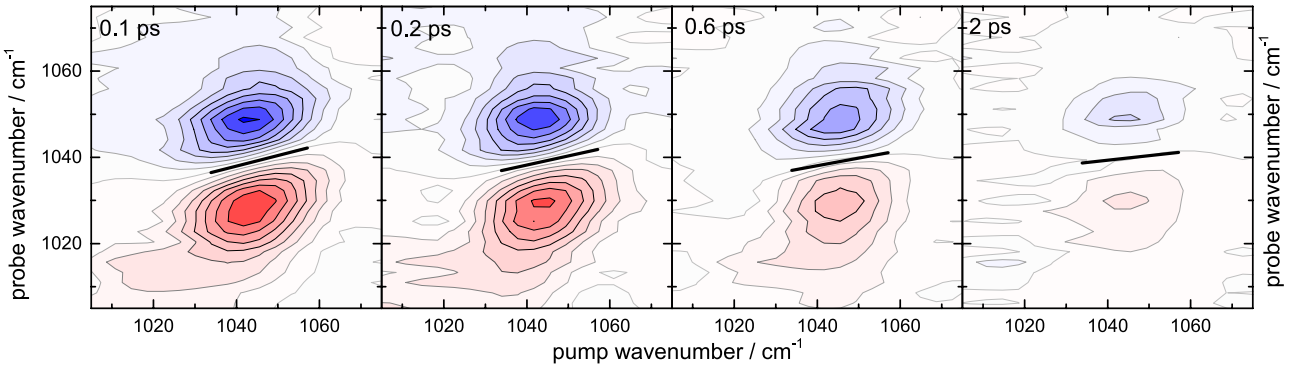

FIG. 2. Sequence of 2D-IR spectra of FACN in D_2O for increasing population times 100 fs, 200 fs, 600 fs, and 2 ps. The thick black lines depict the CLSs. Contour lines are on a linear scale in steps of 10% of the peak amplitude of the 100 fs spectrum.

simulation results, is the small tilt of the line-shapes along the diagonal at early population times. This is the manifestation of an instantaneous inhomogeneous distribution of CF-stretch vibration frequencies, in the sense that the frequency of a given molecule during the pump process is correlated with that during the probe pulse. As the time between both pump and probe processes increases, that correlation gets lost due to spectral diffusion, and the tilt of the 2D-IR line shapes diminishes. A convenient measure of that tilt is the center line slope (CLS) between the 0-1 and the 1-2 peaks in the 2D-IR spectra,[7–9] depicted in Figure 2 as thick black lines. Figure 3(b) shows the decay of the CLS as a function of population time, which characterizes the timescale of spectral diffusion, i.e., the time of the solvent's (re-)orientational dynamics around the solute and possibly the making and breaking of hydrogen bonds of water to the —CF group.

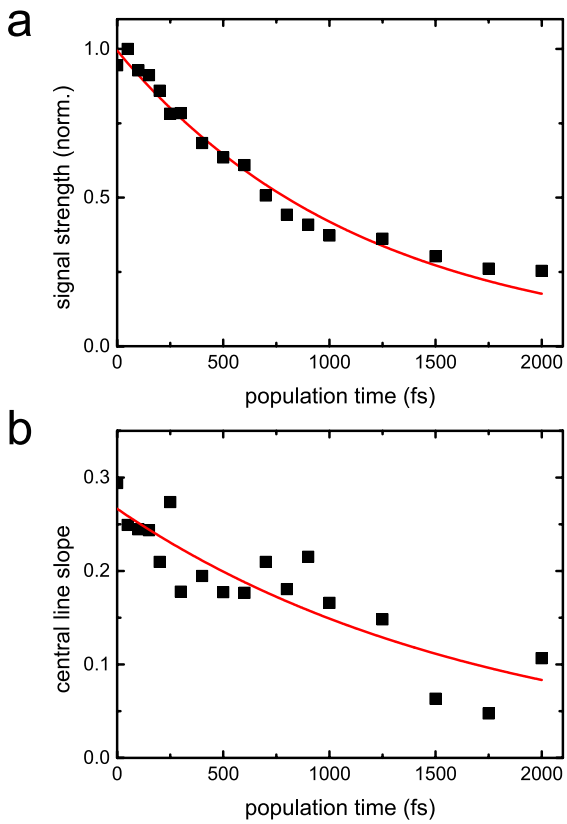

FIG. 3. (a) Decay of the overall signal strength and (b) that of the central nodal slope. In both cases, the data are fit by single exponential functions (red lines), revealing time constants of 1.2 ps for vibrational relaxation and 1.7 ps for spectral diffusion, respectively.

The decay of the CLS is fit to a single-exponential function, which is forced to decay to 0. The fit reveals a time-constant of 1.7 ps for spectral diffusion. It is noted that this number has to be considered an upper limit, as small residual scattering, which generates a spectral feature along the diagonal, might distort the 2D lineshape and generate a fake tilt. That artifact will be in particular relevant at the later delay times around 2 ps when the signal is smallest. Anyhow, the obtained value of 1.7 ± 0.3 ps lies well within the range of what has been observed for other solutes. For example, FFCF decays with 1.3 ps has been observed for N_3^-,[10] 2.9 ps for CN^-,[11] and 1.0–1.6 ps (depending on experiment) for NMA.[13,14]

V. COMPUTATIONAL RESULTS

A. Correlation functions and spectroscopy

Figure 4 reports the FFCFs for the MTP/Morse model (left panel) and the QM/MM simulations with SCC-DFTB together with the frequency distributions $P(\omega)$ obtained from the MD simulation (insets). For the MTP/Morse force field, the frequency distributions (anharmonic) are centered around 1047 cm^{-1}, which is not red shifted compared to the gas phase frequency at 1047 cm^{-1} from a gas phase simulation of the FACN monomer. For PC/Morse, the frequency distribution gives a blue shift of 2 cm^{-1}, and mixed QM/MM simulations at the SCC-DFTB level yield a red shift of 52 cm^{-1}. Experimentally, the CF-stretch frequency in solution is centered around 1040 cm^{-1}, red shifted by 32 cm^{-1} from its gas phase value found at 1071 cm^{-1} and 1073 cm^{-1}, respectively.[55,56] Hence, SCC-DFTB provides a more realistic account of the solvent-induced changes in the CF oscillator frequency.

The FFCFs (Figure 4, main panel) are fit to double (force fields) or triple (SCC-DFTB) exponential decays

$$C(t) = \sum_i a_i \exp(-t/\tau_i) \quad (5)$$

with the parameters summarized in Table II. It is found that the force fields—despite their rather advanced nature in some instances—yield considerably shorter decay

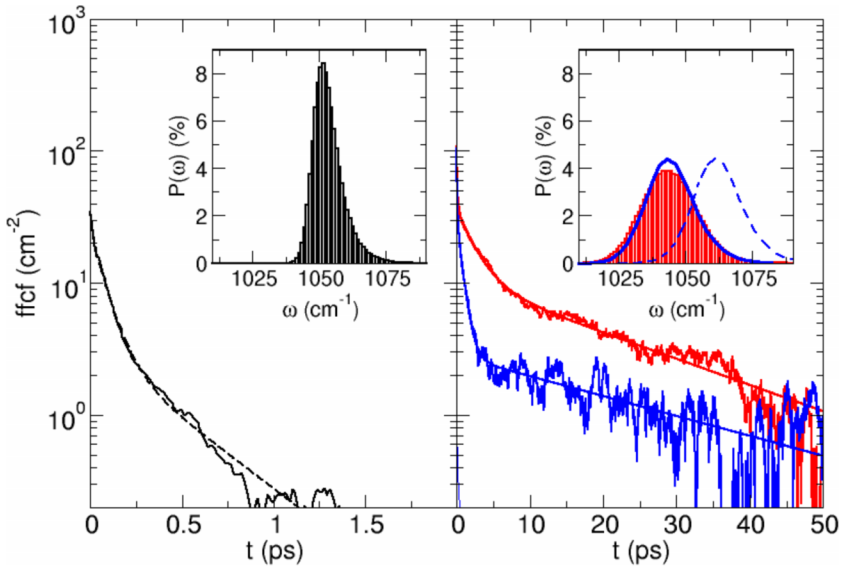

FIG. 4. FFCFs as a function of lag time (solid line) and the corresponding fit (dashed line) for MTP/Morse (left panel) and SCC-DFTB (right panel, red) models. The insets show the corresponding frequency distributions. Note the different time scales in the two panels. The blue line in the right panel is the FFCF based on the MTP/Morse snapshots but frequencies from an SCC-DFTB analysis. The blue trace in the inset is the corresponding frequency distribution (dashed) and the solid line is with the center frequency shifted by −16 cm^{-1} to allow direct comparison of the distribution with the pure SCC-DFTB results.

times than the experimental results. On the other hand, the SCC-DFTB simulations provide quite a realistic account of the experimental FFCF. That is, it shows three time scales with time constants of $\tau_1 = 0.09$ ps, $\tau_2 = 2.4$ ps, and $\tau_3 = 22$ ps. The middle time scale, τ_2, agrees reasonably well with the experimental value, 1.7 ps.

FFCFs of other vibrational chromophores often exhibit a more or less pronounced initial oscillatory contribution, sometimes even leading to anticorrelations at short times. That has been observed, for example, for CN^- in D_2O,[29] HOD in D_2O,[57] or N_3^- in D_2O.[31] In contrast, here the FFCF decays monotonically to zero, similar to what was found for NMA in D_2O.[34] The degree to which such oscillatory features are present in the FFCF at short times has been linked to the strength of the solute-solvent H-bond at the probed oscillator site.[31] As the hydrogen bond strength is expected to decrease in going from CN^-, N_3^-, H_2O, C═O_{NMA} to C—F, the observed behavior in the FFCF would be consistent with such an interpretation. This is also confirmed by electronic structure calculations at the MP2/6-31G(d,p) and MP2/aug-cc-pvtz levels of theory. That is, the strength of the H-bond decreases from −20.5 to −7.0 kcal/mol in going from CN^-–water to FACN–water with N_3^-–water at −17.4 and NMA–water at −9.2 kcal/mol. For MTP/Morse and FPC/Morse, the interaction energies are −4.2 kcal/mol and −9.5 kcal/mol which reduces to −3.5 kcal/mol with SCC-DFTB.

Figure 1 shows the 1D spectra of the FPC (green) and MTP (black) models, deduced from the simulated FFCFs. The FWHMs of these lines are 7 cm^{-1} for FPC/Morse and 6 cm^{-1} for MTP/Morse, respectively, which are narrower than the corresponding frequency distributions (see Figure 4, insets, for MTP/Morse) due to motional narrowing. Hence, both models predict a significantly too narrow line in comparison to experiment (20 cm^{-1}). The difference becomes even more severe when taking into account that the fast T_1 relaxation time of 1.2 ps, which has been included in the calculation of the 1D spectra, contributes about 4 cm^{-1} to the total line width. That is, if one were to compare experimental and simulated spectra after deconvoluting out the T_1 contribution, one would obtain line widths of 16 cm^{-1} versus 2-3 cm^{-1}, respectively. Hence, the force field simulations evidently underestimate the perturbation of the CF-vibrational frequency and possible reasons are discussed further below. On the other hand, the FWHM from SCC-DFTB simulations is 12 cm^{-1}, which is in much better agreement with the experimentally determined data. The maximum of the band also matches the experimental center frequency, which however, is probably a coincidence.

TABLE II. Parameters of a bi-exponential fit of the FFCFs for the different models considered.

	a_1 (cm^{-2})	τ_1 (ps)	a_2 (cm^{-2})	τ_2 (ps)	a_3 (cm^{-2})	τ_3 (ps)
PC/Morse	25.6	0.05	5.5	0.28		
MTP/Morse	24.4	0.05	7.3	0.25		
FPC/Morse	33.6	0.08	6.3	0.43		
SCC-DFTB	58.3	0.09	26.7	2.4	10.5	22

Computed 2D-IR spectra are reported in Figure 5 for the same delay times as the experimental data (Figure 2). The agreement with the experimental 2D-IR spectra is not particularly good for MTP/Morse, which is not overly surprising, given the fact that the simulation already underestimates the line width of the transition. On the other hand, the 2D IR spectra deduced from the SCC-DFTB simulations much more closely resemble the experimental spectra, just like the 1D spectra do. Despite the too narrow line-shapes, however, the CLS can still be evaluated. Their decays are reported in Figure 6, and the results from biexponential fits are summarized in Table III. The resulting time-constants are very similar to the corresponding values form the FFCFs, with the amplitude of the fast component strongly suppressed, since that is strongly in the motional narrowing limit. The similarity of the time constants illustrates the fact that the CLS is a good measure of the FFCF.[7–9] In comparison to experiment, the time-scale of the decay is too fast by roughly a factor of 3 for simulations with an empirical force field, and the CLS is significantly too small as well. This is not the case for the

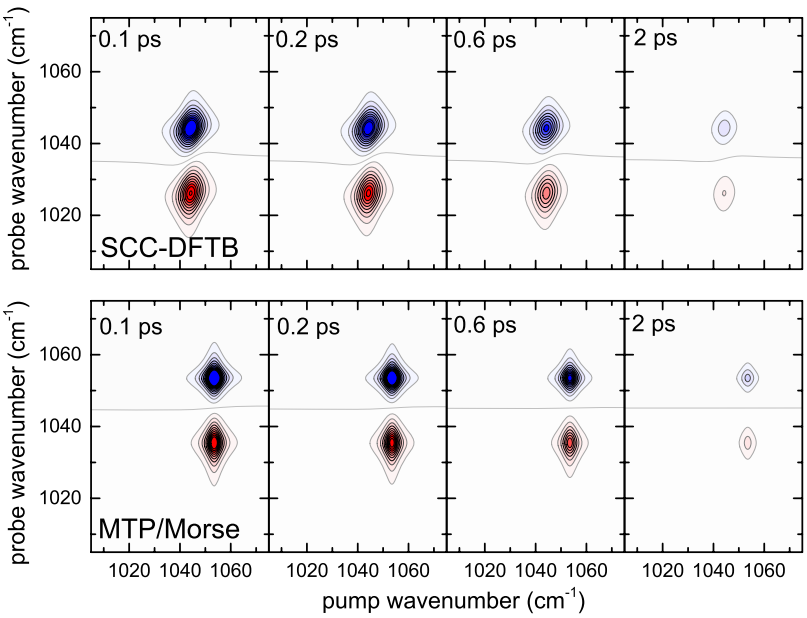

FIG. 5. Simulated 2DIR spectrum of the CF-band of FACN in TIP3P water for SCC-DFTB (top row) and MTP/Morse (bottom row) for increasing population times 100 fs, 200 fs, 600 fs, and 2 ps. Contour lines are on a linear scale in steps of 10% of the peak amplitude of the 100 fs spectrum.

SCC-DFTB simulations for which the decay time and amplitude of the dominant process (τ_2) is in a reasonable agreement with experiment.

An additional account of the SCC-DFTB simulations included the analysis of the structures sampled from MTP/Morse simulations and computing the FFCF at the semi-empirical level, see Figure 4. The decay of the FFCF is reminiscent of the pure SCC-DFTB simulation with decay times of 0.06, 0.75, and 28 ps. Again, the existence of a long time scale is clearly visible although its magnitude is suppressed compared to the full SCC-DFTB QM/MM simulation. The frequency distribution (blue line, inset) closely matches that of the full QM/MM simulation. Hence, despite the different solvent environments in the snapshots (note that the FACN structure is minimized before frequency calculation), the frequency distributions from the QM/MM simulation and the QM-scored MTP/Morse snapshots agree quite closely. Together with the very different frequency distribution from the MTP/Morse simulations this suggests that the bonded terms in the force field may require additional attention.

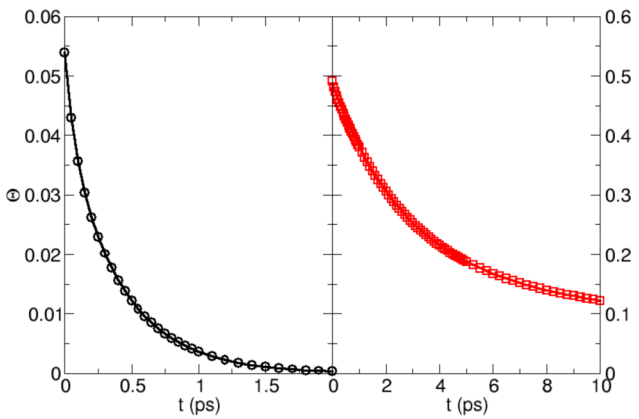

FIG. 6. CLS as a function of the delay time t_2 for FACN in TIP3P for MTP/Morse (left panel) and SCC-DFTB (right panel). The symbols correspond to the data and the lines to the fit which overlap in most cases.

B. Solvent structure around the chromophore

Radial distribution functions (RDFs), $g(r)$ are convenient for characterizing the solvent organization around a solute. To this end, the $g(r)$ for several important distances were analyzed for both FACN and ACN. In the case of FACN, the F–O_W pair distribution function (Figure 7(a), red and black lines) peaks at 3.2 Å and does not differ between MTP/Morse and SCC-DFTB simulations. However, the amplitude (i.e., the occupation probability) is larger for MTP/Morse. This maximum is shifted to larger distances due to the increased van der Waals range of fluorine compared to the hydrogen atoms on the CH_2F group (σ_F = 1.63 Å vs. σ_H = 1.32 Å). For short separations, the H–O_W $g(r)$ from MTP/Morse simulations for FACN (dashed black line in Figure 7(a)) follows closely that for ACN (blue line). However, contrary to ACN the solvent around the hydrogens in FACN still organizes in a shell-like structure (dashed black line in Figure 7(a)).

The most notable feature in the $g_{F-HW}(r)$ involving the water-hydrogen atoms in Figure 7(b) is the weak but clearly manifest hydrogen-bond between the fluoride on the CH_2F-group and the water-hydrogens. It is observable as a clear shoulder around r = 2 Å, which is of about equal size for both the SCC-DFTB and the MTP/Morse simulations (it is a bit more distinct in the case of the SCC-DFTB model). Integration of $g(r)$ yields the occupation number $N_H(r_s)$ of hydrogen atoms as a function of the separation r_s from the fluorine atom. Evaluating $N_H(r_s) = 4\pi\rho_H \int_0^{r_s} r^2 g(r) dr$, with ρ_H the

TABLE III. Fitting parameters for the CLS decay.

	a_1	τ_1 (ps)	a_2	τ_2 (ps)		
MTP/Morse	0.013	0.08	0.04	0.4		
FPC/Morse	0.021	0.08	0.06	0.5		
SCC-DFTB	0.007	0.07	0.32	2.7	0.16	28
Exp.	...	...	0.27	1.7		

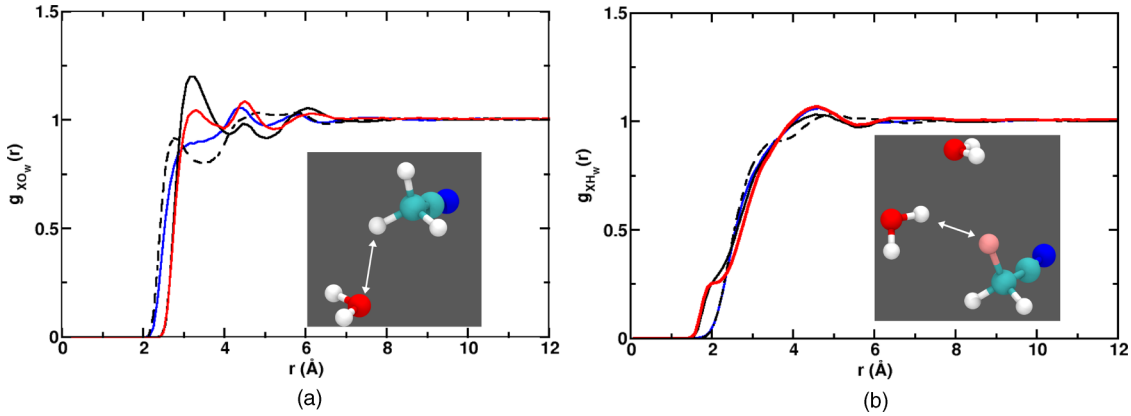

FIG. 7. RDFs for water-ACN and water-FACN. For FACN MTP/Morse (black), for SCC-DFTB (red), and for ACN (blue). Panels (a) and (b) report the $g(r)$ for (a) X–O_W, and (b) X–H_W where X is either F or H on the CFH_2 and CH_3 groups, respectively. The dashed lines in panels (a) and (b) are the H–O_W and H–H_W separations for FACN from MTP/Morse simulations. The insets in panels (a) and (b) illustrate the geometrical coordinates.

hydrogen-density in the simulation system, yields an occupation of 25% at $r_s = 2$ Å. On the other hand, the structuring around the hydrogen atoms of the CFH_2 and CH_3 groups of FACN and ACN, respectively, is very similar at short separations and starts do differ only at ≈4 Å.

VI. SUMMARY

In the present work, the 2-dimensional spectroscopy of fluorinated acetonitrile ($CNCH_2F$, FACN) has been investigated experimentally and through computer simulations. The time scale for spectral diffusion is 1.7 ps from experiment compared with 0.5 ps from force field simulations and 2.4 ps and 22 ps from QM/MM simulations. Although advanced multipolar force fields with van der Waals parameters fitted to experimental data were employed in the simulations, they are unable to quantitatively capture the experimental observations. This is different for the SCC-DFTB simulations which yield a realistic red shift, 1D lineshape and semi-quantitative time scales for the FFCF and the CLS. One reason for the deficiency of the empirical force fields might be that the solvation free energy for FACN is not available as a benchmark to fit the van der Waals parameters. Furthermore, although the bonded parameters in force fields are usually considered as a given, additional refinements of these terms may be necessary for more realistic computations in the present case. For example, couplings between different modes are typically less well controlled because explicit mode-mode coupling terms are not included in a standard force field.

It is interesting to note that for both, FACN (present work) and NMA[34] in water the computed relaxation times of the FFCF from atomistic simulations with a multipolar force field are typically shorter (although to different amounts) than the experimentally determined ones. In both cases, the parametrization of the nonbonded terms proceeded along the same lines and the bonded terms were those from an established force field. Although the oscillator of interest (–CO and –CF) was treated with a Morse potential, accounting for anharmonicity, the computed relaxation times are shorter than the experimentally determined ones. This, together with the result that the frequency distribution $P(\omega)$ from MTP/Morse simulations is considerably narrower at the red, low-frequency side than that from simulations with SCC-DFTB (see Figure 4) further suggests that the bonded terms and in particular their mutual coupling may be a possibility for further improvement. This concerns primarily situations in which the frequency of the oscillator probed in the experiments is in a spectrally denser region as is the case for FACN.

The dynamics found experimentally as well as in the SCC-DFTB simulations is surprisingly slow, while simulations with a multipolar force field are only capable to qualitatively capture the experiments. The semiempirical DFTB simulations provide a realistic description of the spectroscopy and dynamics of the system. In summary, experiment and simulations suggest there to be a reasonably strong hydrogen bond between the fluorine atom of FACN and the surrounding water which could also be of interest in a biological context.

ACKNOWLEDGMENTS

The authors gratefully acknowledge financial support from the Swiss National Science Foundation through Grant No. 200021-117810 (to M.M.) and to the NCCR-MUST (to M.M. and P.H.).

[1]D. Wong, F. Bymaster, and E. Engleman, Life Sci. **57**(5), 411–441 (1995).
[2]B. D. Roth, Prog. Med. Chem. **40**, 1–22 (2002).
[3]K. Drlica and M. Malik, Curr. Top. Med. Chem. **3**(3), 249–282 (2003).
[4]R. Paulini, K. Muller, and F. Diederich, Angew. Chem., Int. Ed. **44**(12), 1788–1805 (2005).
[5]P. Restorp, O. B. Berryman, A. C. Sather, D. Ajami, and J. Rebek, Jr., Chem. Commun. **2009**(38), 5692–5694.
[6]P. Hamm and M. Zanni, *Concepts and Methods of 2D Infrared Spectroscopy* (Cambridge University Press, 2011).
[7]K. Kwac and M. Cho, J. Phys. Chem. A **107**, 5903–5912 (2003).
[8]S. T. Roberts, J. J. Loparo, and A. Tokmakoff, J. Chem. Phys. **125**, 084502 (2006).
[9]K. Kwak, S. Park, I. J. Finkelstein, and M. D. Fayer, J. Chem. Phys. **127**(12), 124503 (2007).
[10]P. Hamm, M. Lim, and R. Hochstrasser, Phys. Rev. Lett. **81**(24), 5326–5329 (1998).
[11]M. Koziński, S. Garrett-Roe, and P. Hamm, Chem. Phys. **341**, 5–10 (2007).

[12]C.-H. Kuo and R. M. Hochstrasser, Chem. Phys. **341**(1-3), 21–28 (2007).
[13]S. Woutersen, R. Pfister, P. Hamm, Y. Mu, D. Kosov, and G. Stock, J. Chem. Phys. **117**(14), 6833–6840 (2002).
[14]M. F. Decamp, L. Deflores, J. M. Mccracken, A. Tokmakoff, K. Kwac, and M. Cho, J. Phys. Chem. B **109**, 11016–11026 (2005).
[15]R. Costard, I. A. Heisler, and T. Elsaesser, J. Phys. Chem. Lett. **5**, 506–511 (2014).
[16]J. B. Asbury, T. Steinel, K. Kwak, S. A. Corcelli, C. P. Lawrence, J. L. Skinner, and M. Fayer, J. Chem. Phys. **121**, 12431–12446 (2004).
[17]S. Yeremenko, M. S. Pshenichnikov, and D. A. Wiersma, Chem. Phys. Lett. **369**, 107–113 (2003).
[18]J. D. Eaves, J. J. Loparo, C. J. Fecko, S. T. Roberts, A. Tokmakoff, and P. L. Geissler, Proc. Natl. Acad. Sci. U. S. A. **102**, 13019–13022 (2005).
[19]F. Perakis and P. Hamm, J. Phys. Chem. B **115**, 5289–5293 (2011).
[20]M. H. Lim, P. Hamm, and R. M. Hochstrasser, Proc. Natl. Acad. Sci. U. S. A. **95**, 15315–15320 (1998).
[21]H. Ishikawa, J. Ilya, S. K. Finkelstein, K. Kwak, J. K. Chung, K. Wakasugi, A. M. Massari, and M. D. Fayer, Proc. Natl. Acad Sci. U. S. A. **104**, 16116–16121 (2007).
[22]J. N. Bandaria, S. Dutta, M. W. Nydegger, W. Rocka, A. Kohen, and C. M. Cheatum, Proc. Natl. Acad. Sci. U. S. A. **107**, 17974–17979 (2010).
[23]G. M. Bonner, A. R. Ridley, S. K. Ibrahim, C. J. Pickett, and N. T. Hunt, Faraday Discuss. **145**, 429–442 (2010).
[24]L. J. G. W. van Wilderen, D. Kern-Michler, H. M. Müller-Werkmeister, and J. Bredenbeck, Phys. Chem. Chem. Phys. **16**, 19643–19653 (2014).
[25]K.-I. Oh, J.-H. Lee, C. Joo, H. Han, and M. Cho, J. Phys. Chem. B **112**, 10352–10357 (2008).
[26]R. Bloem, K. Koziol, S. Waldauer, B. Buchli, R. Walser, B. Samatanga, I. Jelesarov, and P. Hamm, J. Phys. Chem. B **116**, 13705–13712 (2012).
[27]J. T. King and K. J. Kubarych, J. Am. Chem. Soc. **134**, 18705–18712 (2012).
[28]I. Peran, T. Oudenhoven, A. M. Woys, M. D. Watson, T. O. Zhang, I. Carrico, M. T. Zanni, and D. P. Raleigh, J. Phys. Chem. B **118**, 7946–7953 (2014).
[29]M. W. Lee, J. K. Carr, M. Göllner, P. Hamm, and M. Meuwly, J. Chem. Phys. **139**, 054506 (2013).
[30]S. Yang and M. Cho, J. Chem. Phys. **123**(13), 134503 (2005).
[31]S. Li, J. R. Schmidt, A. Piryatinski, C. P. Lawrence, and J. L. Skinner, J. Phys. Chem. B **110**(38), 18933–18938 (2006).
[32]S. Li, J. R. Schmidt, S. A. Corcelli, C. P. Lawrence, and J. L. Skinner, J. Chem. Phys. **124**(20), 204110 (2006).
[33]J.-H. Choi, K.-I. Oh, H. Lee, C. Lee, and M. Cho, J. Chem. Phys. **128**, 134506 (2008).
[34]P.-A. Cazade, T. Bereau, and M. Meuwly, J. Phys. Chem. B **118**(28), 8135–8147 (2014).
[35]P. Hamm, R. A. Kaindl, and J. Stenger, Opt. Lett. **25**, 1798–1800 (2000).
[36]J. Helbing and P. Hamm, J. Opt. Soc. Am. B **28**, 171–178 (2011).
[37]R. Bloem, S. Garrett-Roe, H. Strzalka, P. Hamm, and P. Donaldson, Opt. Express **18**(26), 27067–27078 (2010).
[38]B. R. Brooks, C. L. Brooks III, A. D. Mackerell, Jr., L. Nilsson, R. J. Petrella, B. Roux, Y. Won, G. Archontis, C. Bartels, S. Boresch, A. Caflisch, L. Caves, Q. Cui, A. R. Dinner, M. Feig, S. Fischer, J. Gao, M. Hodoscek, W. Im, K. Kuczera, T. Lazaridis, J. Ma, V. Ovchinnikov, E. Paci, R. W. Pastor, C. B. Post, J. Z. Pu, M. Schaefer, B. Tidor, R. M. Venable, H. L. Woodcock, X. Wu, W. Yang, D. M. York, and M. Karplus, J. Comput. Chem. **30**(10), 1545–1614 (2009).
[39]K. Vanommeslaeghe, E. Hatcher, C. Acharya, S. Kundu, S. Zhong, J. Shim, E. Darian, O. Guvench, P. Lopes, I. Vorobyov, and A. D. Mackerell, Jr., J. Comput. Chem. **31**(4), 671–690 (2010).
[40]W. L. Jorgensen, J. Chandrasekhar, J. D. Madura, R. W. Impey, and M. L. Klein, J. Chem. Phys. **79**, 926–935 (1983).
[41]W. V. Gunsteren and H. Berendsen, Mol. Phys. **34**, 1311–1327 (1977).
[42]S. E. Feller, Y. Zhang, R. W. Pastor, and B. R. Brooks, J. Chem. Phys. **103**, 4613–4621 (1995).
[43]M. P. Allen and D. J. Tildesley, *Computer Simulation of Liquids* (Oxford University Press, New York, 1987).
[44]T. Bereau, C. Kramer, and M. Meuwly, J. Chem. Theory Comput. **9**(12), 5450–5459 (2013).
[45]C. Kramer, P. Gedeck, and M. Meuwly, J. Comput. Chem. **33**, 1673–1688 (2012).
[46]T. Bereau, C. Kramer, F. W. Monnard, E. S. Nogueira, T. R. Ward, and M. Meuwly, J. Phys. Chem. B **117**(18), 5460–5471 (2013).
[47]U. Koch, P. L. A. Popelier, and A. J. Stone, Chem. Phys. Lett. **238**(4-6), 253–260 (1995).
[48]C. Kramer, T. Bereau, A. Spinn, K. R. Liedl, P. Gedeck, and M. Meuwly, J. Chem. Inf. Model. **53**(12), 3410–3417 (2013).
[49]D. R. Nutt and M. Meuwly, Biophys. J. **85**, 3612–3623 (2003).
[50]D. R. Nutt and M. Meuwly, ChemPhysChem **5**, 1710–1718 (2004).
[51]M. Elstner, D. Porezag, G. Jungnickel, J. Elsner, M. Haugk, T. Frauenheim, S. Suhai, and G. Seifert, Phys. Rev. B **58**, 7260–7268 (1998).
[52]Q. Cui, M. Elstner, E. Kaxiras, T. Frauenheim, and M. Karplus, J. Phys. Chem. B **105**, 569–585 (2001).
[53]T. Kuba, Z. Bodrog, M. Gaus, C. Khler, B. Aradi, T. Frauenheim, and M. Elstner, J. Chem. Theory Comput. **9**(7), 2939–2949 (2013).
[54]S. Mukamel, *Principles of Nonlinear Optical Spectroscopy* (Oxford University Press, 1999).
[55]R. Jones and W. Orville-Thomas, J. Chem. Soc. **207**, 4632–4646 (1965).
[56]A. Baldacci, P. Stoppa, A. Charmet, and S. Giorgianni, J. Mol. Spectrosc. **207**(1), 32–38 (2001).
[57]K. B. Møller, R. Rey, and J. T. Hynes, J. Phys. Chem. A **108**, 1275–1289 (2004).
[58]See supplementary material at http://dx.doi.org/10.1063/1.4916630 for the results from FTIR and NMR spectroscopy and summarizes the MTP parametrization derived from fitting to the condensed phase properties together with the MM3 parameters used for the bond, angle, and bond-angle parameters.